TOWARDS BETTER CORRELATION BETWEEN OPTICAL AND COMMERCIAL SPARK IGNITION ENGINES THROUGH QUASI-DIMENSIONAL MODELING OF CYCLE-TO-CYCLE VARIABILITY

by

Adrian IRIMESCU**, Simona Silvia MEROLA, and Bianca Maria VAGLIECO

CNR Istituto Motori, Naples, Italy

Original scientific paper
https://doi.org/10.2298/TSCI200511333I

Internal combustion engines are still the main choice when considering propulsion technology in the transport sector. Spark ignition units offer the advantage of good efficiency with simpler after-treatment systems. Lean operation is a promising strategy that would further improve efficiency, but requires mitigation of cycle-to-cycle variability. Within this context, and given the increasing trend of using simulation based evaluations during engine development, the current work investigated combustion in an optical spark ignition engine through measurements and quasi-dimensional simulation. The possibility of visualizing in-cylinder processes provides unique insight, but also introduces complications with respect to commercial engines. For this reason, quasi-dimensional simulation was applied so as to better understand the factors that induce cycle-to-cycle variability. For the specific case of the investigated engine, cycle-to-cycle measured exhaust air-fuel ratio was found to be directly correlated to variations of engine output. Several routes of incorporating these effects into simulations were evaluated. Introducing a random component in the period of laminar-turbulent flame transition was found to ensure good grounds for simulating peak pressure variability. Indicated mean effective pressure on the other hand was found to depend less on the initial stages of combustion and was strongly correlated to aforementioned variability of exhaust air-fuel ratio.

Key words: *spark ignition engine, quasi-dimensional simulation, optical accessibility, cycle-to-cycle variability*

Introduction

Fuel conversion efficiency of spark ignition (SI) engines has been continuously improved, together with consistent reduction of their environmental impact [1]. One of the main challenges to be faced is that abnormal combustion phenomena limit peak output due to possible engine damage, as well as the maximum compression ratio that can be used [2]. It is therefore essential to identify appropriate control strategies to avoid knocking. Direct injection (DI) provides higher flexibility in this respect [3, 4] and combined with other systems such as water delivery to the intake manifold [5] or octane-on-demand concepts [6] can ensure high output with increased efficiency.

Given the inherent stochastic nature of knocking, the ability to model cycle-to-cycle variability (CCV) can represent an important advantage when applying quasi-dimensional

* Corresponding author, e-mail: a.irimescu@im.cnr.it

simulation. Such approaches feature a good compromise between accuracy and computational effort [7]. They are not as fast as ANN based models [8] but can ensure acceptable fast-running characteristics [9] and several levels of detail can be implemented for augmenting predictive capabilities [10, 11]. Data recorded on optically accessible units can ensure a solid starting point for model development and validation, as they feature high spatial resolution [12, 13]. They also provide an opportunity of better identifying the effects of mass transfer of unburned charge from the top-land region to the combustion chamber late during expansion. This phenomenon can feature flame penetration into the aforementioned crevice [14, 15] and may induce auto-ignition prone regions in the next cycle, thus partially explaining observed multi-cycle specifics of low-speed pre-ignitions [16].

Within this context, the present work looked at experimental data recorded on an optical DISI engine and quasi-dimensional modeling of combustion was applied, with a focus on CCV. A semi-empirical approach was taken, by first introducing a random variation of the coefficient that controls the simulation of the initial combustion stage, during the transition from laminar to the turbulent flame regime. Correlation of engine output to exhaust air-fuel ratio variations were also scrutinized. Apart from providing a tool for detailed analysis, quasi-dimensional simulation can help with better correlation of data recorded on optical engines and measurements performed on commercial units. More to the point, operating conditions specific for real-world use can be simulated in different points of the speed-load map that cannot be investigated due to design limitations imposed by the transparent window. As a result of this approach, a solid starting point can be provided for developing control strategies that are relevant for commercial engines, with the advantage of better identification of phenomena through optical techniques.

Materials and method

Experimental data

An experimental DISI power unit was used for performing the trials. Optical accessibility was ensured through the piston crown, with a Bowditch design [17], fig. 1. Main engine specifications are listed in tab. 1.

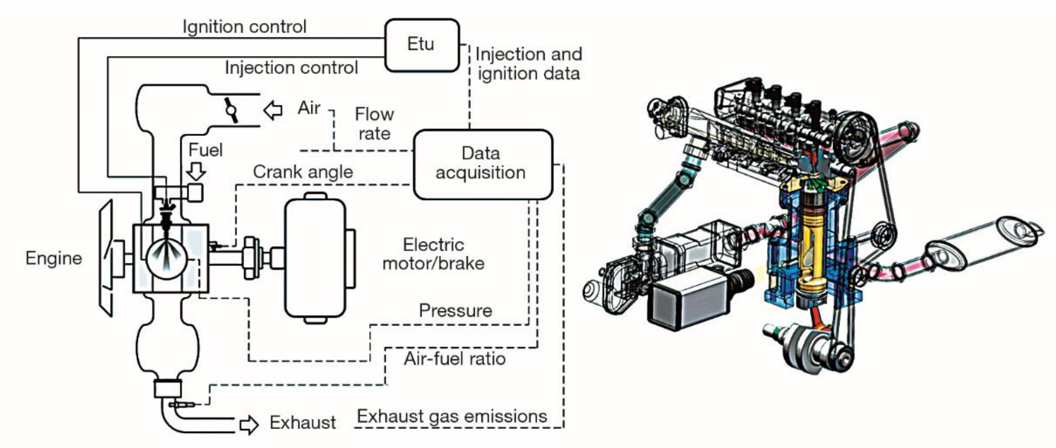

Figure 1. Experimental set-up and schematic representation of acquired signals [18]

Please note that throughout the text reference will be made to the firing TDC unless otherwise specified. References [19, 20] contain detailed description of the measurement procedure, as well as post-processing techniques [13].

In brief, the data was recorded during engine operation at 2000 rpm, wide open throttle and 12° bTDC spark timing. Injection pressure was set at 100 bar and fuel delivery timing was 290° bTDC. In-cylinder pressure constituted the main parameter of interest and it was recorded with an accuracy of ±1% and resolution of 0.2°. Other values such as intake pressure, temperature, air-fuel ratio (AFR) were also used as boundary conditions for the simulation. Data was averaged over 200 consecutive cycles, with identification of peak pressure, indicated mean effective pressure (IMEP) and exhaust lambda evaluated on a cycle-to-cycle basis as well.

Table 1. Engine specifications

Bore × stroke	79 × 81.3 mm
Connecting rod length	143 mm
Cylinders	1
Compression ratio	10:1
IVO	3° bTDC
IVC	36° aBDC
EVO	27° bBDC
EVC	0° aTDC
Fuel system	Wall guided direct injection

Simulation model

A complete numerical model (containing the intake and exhaust system) was built in the GT-POWER simulation framework [21]. More detailed information on the model and its calibration procedure can be found in [22]. Just to better illustrate the procedure related to CCV modeling, eqs. (1)-(4) are shown, as they constitute the core of the combustion submodel:

$$S_{\mathrm{T}} = C_{\mathrm{TFS}} u' \left[1 - \frac{1}{1 + C_{\mathrm{FKG}} \left(\frac{R_{\mathrm{f}}}{L_{\mathrm{i}}} \right)^2} \right] \tag{1}$$

$$\frac{\mathrm{d}M_{\mathrm{b}}}{\mathrm{d}t} = \frac{M_{\mathrm{e}} - M_{\mathrm{b}}}{\tau} \tag{2}$$

$$\frac{\mathrm{d}M_{\mathrm{e}}}{\mathrm{d}t} = \rho_{\mathrm{u}} A_{\mathrm{e}} (S_T + S_L) \tag{3}$$

$$\tau = \frac{\lambda_{\mathrm{T}}}{S_L} \tag{4}$$

where S_T [ms^{-1}] is the turbulent flame speed, u' [ms^{-1}] – the turbulence intensity, R_f [m] – the flame radius and L_i [m] – the integral length scale, M_b [kg] – the burned mass, M_e [kg] – the entrained mass, τ [s] – the burn-up time, ρ_u [kgm^{-3}] – the unburned gas density, A_e [m^2] – the flame front surface area, S_L [ms^{-1}] – the laminar flame speed, and λ_T [m] – the Taylor length scale.

There are three calibration coefficients, namely C_TFS for the turbulent flame speed, C_FKG for the flame kernel growth (FKG) phase and C_TLS for the Taylor length scale (working as a proportionality factor between λ_T and L_i). Larger values for the first two result in faster charge entrainment, and lower values for the third coefficient predict higher burn rates *via* eqs. (2) and (4). A detailed discussion on how these calibration parameter were handled is presented in the ensuing section.

The main difference with respect to the previous version of the model [22] is that two random signal generators were added, one for the FKG parameter and the other for the fuel delivery rate of the DI component. This essentially means that for CCV simulations, the initial stages of combustion (*i.e.* the transition from laminar to turbulent) featured random C_FKG values, and casual injected fuel quantity was modeled with uniform distribution of generated numbers. The two signal generators are highlighted with dashed lines in fig. 2. Perturbations were used in the *injector-DI* component and within the combustion sub-model (*i.e.* even if the signals were not directly connected to the corresponding components). The range of random values was chosen based on experimental data, as it will be evident later on in the text.

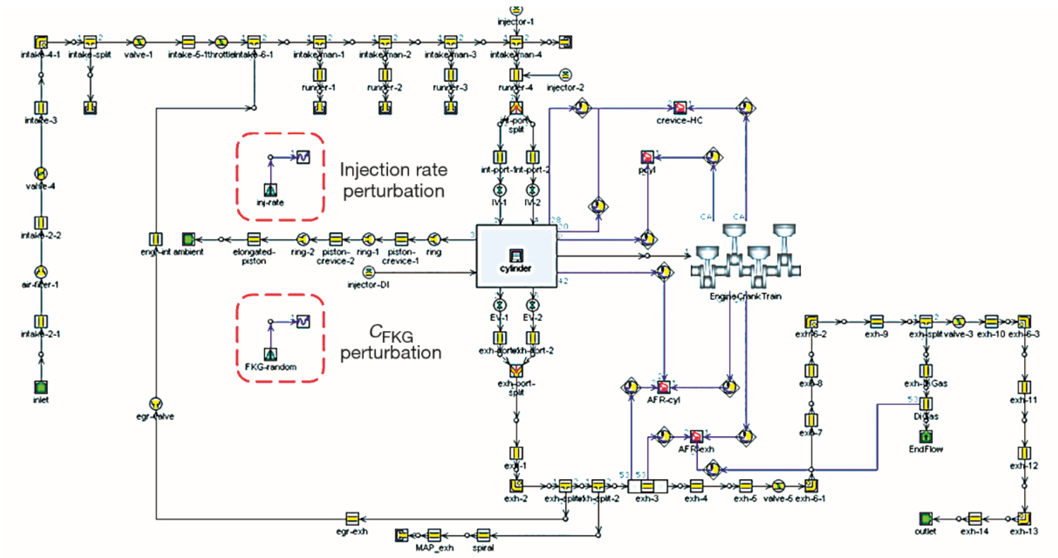

Figure 2. Overview of the engine model, with the two signal generators highlighted with dashed lines

Results and discussion

As mentioned in the experimental part, the investigated condition was at 2000 rpm, close to stoichiometric fueling with gasoline. This resulted in a net indicated mean effective pressure (IMEP) of 7.7 bar, with a coefficient of variation, COV_imep, of 1.8%. One of the first actions that was taken when calibrating the model was to match the average experimental air and fuel flow values. Using the motored pressure traces as a starting point, the compression ratio (CR) and blow-by area, A_{bb}, were determined. Crevice volume, V_{cr}, plays an essential role for optical engines, and this sub-model was set so as to obtain a simulated IMEP within 5% of the measured value. Figure 2 shows the optimized calibration parameters and resulting pressure trace compared to that averaged over 200 consecutive cycles.

The actual compression ratio used in the simulation was found to be higher than the geometric value listed in tab. 1. This is due to a slight increase given the piston expansion effects, but also to compensate for the relatively large V_{cr} value required for correct simulation of IMEP (*i.e.* using the V_{cr} determined based on geometric dimensions of the top-land region height and piston-cylinder clearance value of around 3 cm^3 resulted in predicted IMEP of over 8.9 bar compared to 8.1 bar for the case shown in fig. 3).

The C_{TFS} and C_{TLS} coefficients were calibrated so as to best match the pressure trace from ignition to its peak value. It should be noted that default values are 1. For the C_{FKG} parameter, there is a limitation given by the non-linear influence it has on S_T. Figure 4 illustrates the evolution of the FKG function for a range of C_{FKG} between 0 and 2. The trace was obtained by considering an average integral length, L_i, of 0.2 of the bore, B, and the instance where the flame reaches the cylinder, r_f = B/2. Another constraint is that its minimum value needs to be 0.1 (imposed by the simulation code). As a result, the range that was chosen for the random generation of FKG multiplier values during the simulation was between 0.10 and 1.00, with 0.35 (marked with a circle in fig. 3) used for the calibration of C_{TFS} and C_{TLS} based on the pressure trace averaged over 200 consecutive cycles (the case illustrated in fig. 3).

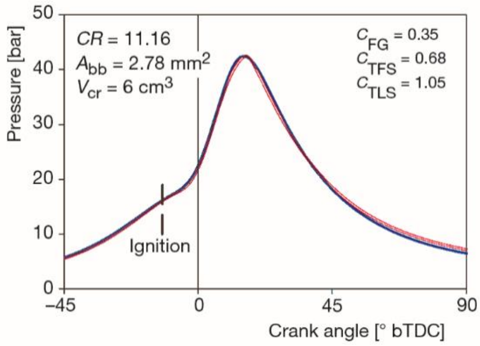

Figure 3. Measured (single line) and simulated (double line) in-cylinder pressure; TDC and ignition crank angles are marked with vertical lines

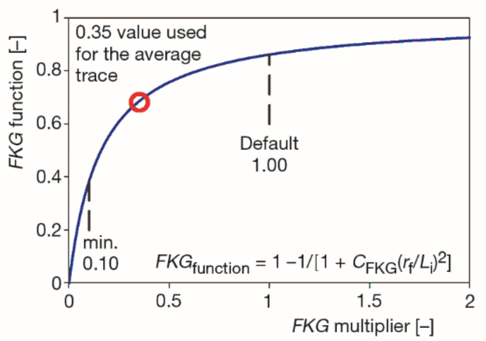

Figure 4. Flame kernel growth function for a range of C_{FKG} values

In more recent versions of the GT-POWER software, there are several options for simulating CCV. They range from introducing a standard distribution of changes in the laminar flame speed and flame kernel growth multiplier (with a typical value around 0.5) to simply changing the standard deviation of C_{TFS} and C_{TLS}. More complex models include perturbation of the instance when combustion starts after spark timing [23]. Several correlations were identified between different factors that influence CCV, but the main conclusion was that local flow and turbulence characteristics play the most important role [24, 25]. Rather than using built-in CCV sub-models, the present work took a more fundamental oriented approach, by looking at ways to closely identify the sources of variability in the investigated optical engine.

With this in mind, and considering that major changes in the flame-turbulence interactions are most likely during the kernel phase, it was chosen to use the random generation of C_{FKG} values as the main source of cycle-to-cycle variations. The assumption was also based on the fact that once the flame radius exceeds the integral length scale, it is exposed to the entire turbulence spectrum and can thus be considered as fully turbulent [26].

Once the range of C_{FKG} was determined, simulations were performed for the minimum, intermediate and maximum values (*i.e.* 0.10, 0.35, and 1.00). Figure 5 shows the results for the three cases, with measured traces chosen for three cycles out of the set of 200, with lowest (designated as low) and highest (fast) peak pressure, as well as the trace closest to the average one (avg). It should be noted that only C_{FKG} was changed, while all other parameters were kept the same.

As quite evident from the graph, only the trace closest to the average (case avg) featured acceptable prediction during the flame propagation phase (*i.e.* from ignition to peak pressure). All three cases were found to calculate lower pressure values during the expansion stroke. This is further evidenced by measured IMEP values of 7.64, 7.70, and 7.86 bar for the slow-avg-fast cases, compared to simulated figures of 8.10, 8.13, and 8.13, respectively. Nonetheless, it can stated that even with a relatively contained modification of the quasi-dimensional model, the effects of CCV in terms of peak pressure variation could be modeled as direct consequence of the interaction between the flame and turbulence during kernel growth. The fact that this was approached in a semi-empirical way (*i.e.* by implementing an assumption based on the size of the kernel) can be seen as an encouraging result.

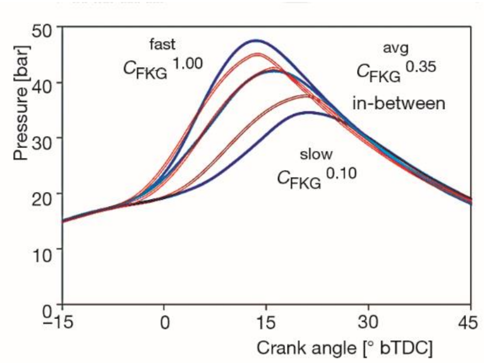

Figure 5. Measured (single lines) and simulated (double lines) for the three cases (slow-avg-fast) with defined C_{FKG} values

One observation is that a relatively weak correlation was found between measured peak pressure and IMEP values; for the set of 200 cycles that was investigated, the linear correlation featured an R^2 value below 0.19. Together with the three aforementioned simulated IMEP values, this observation suggests that further improvements could be looked for. When plotting the IMEP-equivalence ratio points for the set of experimental data, an interesting correlation emerges (fig. 6: equivalence ratio was preferred to lambda values, given the direct correlation with heat input). By considering the response time of the AFR sensor, the corresponding trace was shifted by three cycles and this compares well to the average time lag of lambda sensors of around 0.3 seconds [22]. To put things into perspective, an entire cycle lasts about 60 ms at 2000 rpm, and the mentioned average response time is equivalent to about 5 cycles. After the shift, an inversely proportional correlation coefficient R^2 of 0.64 was found between measured lambda and instant engine output. This fits well with the direct correlation between heat input and IMEP. Based on the observed variation of the signal given by the lambda sensor, an additional random perturbation was introduced *via* the injection rate of the DI component. Based on the minimum and maximum lambda value, a range of injection rate was defined and a corresponding random signal generator was added to the model.

Figure 7 shows the results of simulated 200 consecutive cycles superimposed on lines that define the range of measured data. The FKG designates points for which only the C_{FKG} parameter was random, while AFR includes air-fuel ratio variations as well.

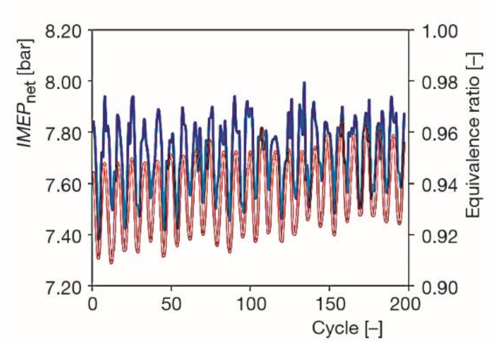

Figure 6. Measured IMEP (single line) and equivalence ratio (double line) for the 200 consecutive cycles; the last three cycles are not shown, given the need for shifting the air-fuel ratio data

As the peak pressure data shows, the variation of this parameter can be relatively well modeled with the introduction of perturbations in the duration of the initial stage of combustion. There is some influence of the air-fuel ratio, but it can be seen as minor compared to the effects of FKG. Another interesting observation is that the actual shape of the function shown in fig. 4 induces a bias of simulated peak pressure values towards the higher range. The distribution of experimental data was more uniform, but also slightly biased towards the upper part of the interval. Randomly changing only the FKG parameter resulted in practically insignificant variations of simulated IMEP. This is emphasized by the symbols (diamond shaped in fig. 7, middle) that overlay the measurement average line. Adding the AFR disturbance resulted in quite good match between the numerical IMEP spread and the range defined by the standard deviation of measured values. Predicted AFR (taken as the real time variable *effec-*

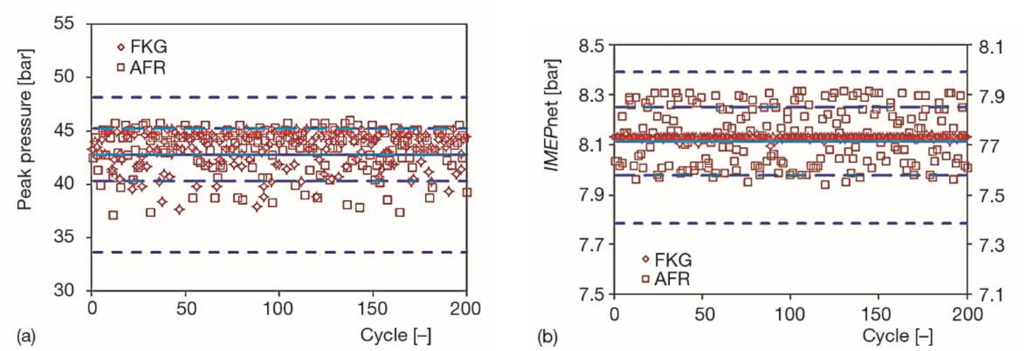

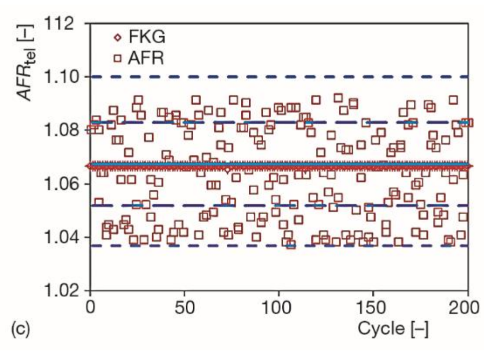

Figure 7. Measured (lines) and simulated (symbols) peak pressure (top), IMEP (middle) and relative AFR (bottom) values for 200 consecutive cycles; for experimental only ranges of data are shown, as average (continuous line), standard deviation (dashed lines) and extreme (dotted lines) minimum-maximum

tive lambda at EVO, updated once per cycle) also confirms the influence this parameter has on IMEP, with very similar distribution of the points obtained for the FKG and AFR simulation cases.

One issue is that the linear correlation between numerical IMEP and lambda values featured an R^2 of over 0.99, much higher than the experimental figure of 0.64. This further emphasizes that other than the initial stages of combustion, there are additional important factors of influence with respect to engine output. Nonetheless, the fact that introducing changes in the fuel flow rate correctly predicted that range of IMEP CCV, together with the experimental lambda values, suggest that the main phenomena can be captured by the approach.

A possible explanation is that pressure oscillations within the fuel rail, combined with the response of the pressure regulating circuit, could result in modifications of injection rates. This is further backed by the fact that modifications of volumetric efficiency are unlikely, given that air intake features relatively high reproducibility, as does the exhaust process. When looking at the oscillations of the lambda signal shown in fig. 6, one possible influence is that pressure waves and related cyclic phenomena could result in modifications of the residual gas present at the end of exhaust. Such changes, on the other hand, cannot explain the extensive range of data recorded *via* the lambda sensor (*e.g.* pressure at intake TDC was found to be within a ±6% range compared to the average, thus resulting in much more contained variations of residual gas, equivalent to less than 1% changes in overall fresh charge mass).

One other phenomenon that could influence IMEP is related to changes in the oxidation efficiency due to the aforementioned large top-land region volume. Further development of the crevice sub-model could therefore provide significant improvement of predictive capabilities with respect to combustion efficiency. Oxidation in *chemical kinetics mode* (as opposed to flame related entrainment and burn-up processes) in the crevice volume even after EVO could be a solid starting ground for predicting cyclic behavior, and may ensure significant advantages when undertaking the previously mentioned situations of simulating knocking events. Nonetheless, the chosen approach is a simple way of directly relating actual heat input to the phenomena that result in IMEP variations.

An essential aspect is that the approach is semi-empirical, meaning that it started with the assumption that the influence on flame front propagation is most likely to be exerted during the kernel development phase. Also, the range in which AFR values were randomly varied was chosen based on measurements with a lambda sensor, therefore not directly related to experimental IMEP values. Of course, one of the main aspects to be further investigated is the ability to model CCV in a wide range of operating conditions.

Conclusions

Data recorded on an optically accessible SI engine was used for evaluating ways to simulate combustion variability in a quasi-dimensional framework. Starting from fundamental considerations, random variations were introduced in the flame kernel growth multiplier. As further development, promising results could be obtained by identifying ways to more closely correlate the range of flame kernel growth coefficient values to the characteristics of flame–turbulence interaction. The range of changes in the injection rate was chosen based on cycle-to-cycle lambda values measured at the exhaust.

One of the main conclusions is that changes in the flame kernel growth multiplier could correctly simulate peak pressure extremes (*i.e.* the range of standard deviation from the average of the recorded 200 consecutive cycles). Engine output on the other hand was found to be less correlated to peak pressure variations, but more directly linked to heat input. In fact, the random changes in the injection rate was found to correctly predict the standard deviation range of IMEP.

These findings identified ways of improving CCV modeling capabilities when undertaking the simulation of combustion related processes in optically accessible SI engines. The correlation of engine output to combustion efficiency is an interesting research opportunity in the special case of optical units, and was designated as the most promising route for future development. Associated improvement of crevice sub-models needs to be of high priority, given that these volumes play an important role in the processes that influence overall oxidation efficiency and have high potential of ensuring a route for modeling multi-cycle characteristics of pre-ignition events.

Acknowledgment

The authors thank for the support of Carlo Rossi and Bruno Sgammato in the experimental activity.

References

[1] Alagumalai, A., Internal Combustion Engines: Progress and Prospects, *Renew. Sust. Energ. Rev.*, *38* (2014), Oct., pp. 561-571
[2] Heywood, J. B., *Internal Combustion Engine Fundamentals*, McGraw Hill, New York, USA, 1988
[3] Wang, Z., *et al.*, Knocking Combustion in Spark-Ignition Engines, *Progress Energ. Combust. Sci.*, *61* (2017), July, pp. 78-112
[4] Singh, E., *et al.*, Optimizing Split Fuel Injection Strategies to Avoid Pre-Ignition and Super-Knock in Turbocharged Engines, *Int. J. Engine Res.*, *22* (2019), 1, pp. 199-221
[5] Zembi, J., *et al.*, CFD Analysis of Port Water Injection in a GDI Engine under Incipient Knock Conditions, *Energies*, *12* (2019), 18, 3409
[6] Singh, E., *et al.*, Knock and Pre-Ignition Limits on Utilization of Ethanol in Octane-on-Demand Concept, SAE Technical Paper 2019-24-0108, 2019
[7] Verhelst, S., Sheppard, C. G. W., Multi-Zone Thermodynamic Modelling of Spark-Ignition Engine Combustion – An overview, *Energ. Convers. Manage.*, *50* (2009), 5, pp. 1326-1335
[8] Tosun, E., *et al.*, Estimation of Operational Parameters for a Direct injection Turbocharged Spark Ignition Engine by Using Regression Analysis and Artificial Neural Network, *Thermal Science*, *21* (2017), 1B, pp. 401-412
[9] Wang, S., *et al.*, A Real-Time Model for Spark Ignition Engine Combustion Phasing Prediction, *SAE Int. J. Engines*, *9* (2016), 2, pp. 1180-1190
[10] Sjeric, M., *et al.*, Development of a Two Zone Turbulence Model and its Application to the Cycle-Simulation, *Thermal Science*, *18* (2014), 1, pp. 1-16
[11] Gan, H., *et al.*, Investigation of the Miller Cycle on the Performance and Emission in a Natural Gas-Diesel Dual-Fuel Marine Engine by Using Two Zone Combustion Model, *Thermal Science*, *24* (2020), 1A, pp. 259-270
[12] Aleiferis, P. G., *et al.*, Integral Length Scales and Time Scales of Turbulence in an Optical Spark-Ignition Engine, *Flow Turb. Combust.*, *98* (2017), 2, pp. 523-577
[13] Martinez, S., *et al.*, Flame Front and Burned Gas Characteristics for Different Split Injection Ratios and Phasing in an Optical GDI Engine, *Appl. Sci.*, *9* (2019), 3, 449
[14] Janas, P., *et al.*, Penetration of the Flame Into the Top-Land Crevice – Large-Eddy Simulation and Experimental High-Speed Visualization, SAE Technical Paper 2015-01-1907, 2015
[15] Penaranda, A., *et al.*, Characterization of Flame Front Propagation During Early and Late Combustion for Methane-Hydrogen Fueling of an Optically Accessible SI Engine, *Int. J. Hydrogen Energ.*, *43* (2018), 52, pp. 23538-23557
[16] Kalaskar, V., *et al.*, Impact of Engine Age and Engine Hardware on Low-Speed Pre-Ignition, SAE Technical Paper 2018-01-1663, 2018
[17] Bowditch, F., A New Tool for Combustion Research A Quartz Piston Engine, SAE Technical Paper 610002, 1961

[18] Merola, S. S., *et al*., Effect of Fuel Injection Strategy on the Carbonaceous Structure Formation and Nanoparticle Emission in a DISI Engine Fuelled with Butanol, *Energies*, *10* (2017), 7, 832
[19] Irimescu, A., *et al*., Application of an Entrainment Turbulent Combustion Model with Validation Based on the dIstribution of Chemical Species in an Optical Spark Ignition Engine, *Appl. Energ., 162* (2016), Jan., pp. 908-923
[20] Irimescu, A., *et al*., Evaluation of Compression Ratio and Blow-By Rates for Spark Ignition Engines Based on In-Cylinder Pressure Trace Analysis, *Energ. Convers. Manage.*, *162* (2018), Apr., pp. 98-108
[21] ***, Gamma Technologies, GT-SUITE Flow Theory Manual Version 7.4, 2013
[22] Irimescu, A., Back-Pressure and Fuel Type Effects on Exhaust Gas Oxygen Sensor Readings for a Single Cylinder Spark Ignition Engine Running on Gasoline and Ethanol, SAE Technical Paper 2019-24-0046, 2019
[23] Wenig, M., *et al*., A New Approach for Modeling Cycle-to-Cycle Variations within the Framework of a Real Working-Process Simulation, *SAE Int. J. Engines*, *6* (2013), 2, pp. 1099-1115
[24] Vitek, O., *et al*., Modeling Cycle-to-Cycle Variations in 0-D/1-D Simulation by Means of Combustion Model Parameter Perturbations based on Statistics of Cycle-Resolved Data, *SAE Int. J. Engines*, *6* (2013), 2, pp. 1075-1098
[25] Schiffmann, P., *et al*., Empirical Investigation of Spark-Ignited Flame-Initiation Cycle-to-Cycle Variability in a Homogeneous Charge Reciprocating Engine, *Int. J. Engine Res.*, *19* (2018), 5, pp. 491-508
[26] Kosmadakis, G. M., *et al*., CFD-Based Method with an Improved Ignition Model for Estimating Cyclic Variability in a Spark-Ignition Engine Fueled with Methane, *Energ. Convers. Manage.*, *174* (2018), Oct., pp. 769-778

Paper submitted: May 11, 2020
Paper revised: October 5, 2021
Paper accepted: October 9, 2021